

## Article

# Development and Applications of an In Situ Probe for Multi-Element High-Resolution Measurement at Soil/Sediment-Water Interface and Rice Rhizosphere

Meng Zhao <sup>1,2,3,†</sup>, Jiang Liu <sup>1,2,†</sup>, Chuangchuang Zhang <sup>1,2</sup>, Xuefeng Liang <sup>2</sup>, Qian E <sup>1,2</sup>, Rongle Liu <sup>2</sup>, Yujie Zhao <sup>1,2,\*</sup> and Xiaowei Liu <sup>1,2,\*</sup>

- <sup>1</sup> Key Laboratory for Environmental Factors Control of Agro-Product Quality Safety, Ministry of Agriculture and Rural Affairs, Tianjin 300191, China; 82101181137@caas.cn (M.Z.); 15548810038@163.com (J.L.); chuangchuangzhang@126.com (C.Z.); eqian1993@126.com (Q.E.)
- <sup>2</sup> Agro-Environmental Protection Institute, Ministry of Agriculture and Rural Affairs, Tianjin 300191, China; liangfxuefeng@caas.cn (X.L.); liurongle@caas.cn (R.L.)
- <sup>3</sup> Institute of Plant Nutrition, Resources and Environment, Beijing Academy of Agriculture and Forestry Sciences, Beijing 100097, China
- \* Correspondence: zhaoyujie@caas.cn (Y.Z.); xwliu2006@163.com (X.L.)
- † These two authors contributed equally to this work.



**Citation:** Zhao, M.; Liu, J.; Zhang, C.; Liang, X.; E, Q.; Liu, R.; Zhao, Y.; Liu, X. Development and Applications of an In Situ Probe for Multi-Element High-Resolution Measurement at Soil/Sediment-Water Interface and Rice Rhizosphere. *Agronomy* **2021**, *11*, 2383. <https://doi.org/10.3390/agronomy11122383>

Academic Editor: Stefano Cesco

Received: 14 October 2021

Accepted: 15 November 2021

Published: 24 November 2021

**Publisher's Note:** MDPI stays neutral with regard to jurisdictional claims in published maps and institutional affiliations.



**Copyright:** © 2021 by the authors. Licensee MDPI, Basel, Switzerland. This article is an open access article distributed under the terms and conditions of the Creative Commons Attribution (CC BY) license (<https://creativecommons.org/licenses/by/4.0/>).

**Abstract:** The biogeochemistry of multi-elements, such as sulfur (S), phosphorus (P) and arsenic (As), is interlinked especially at interfaces of soil/sediment–water and plant rhizosphere. To explore the biogeochemical behavior of multi-elements such as S–P–As at interfaces, an in situ and high-resolution technology is required. In this study, we developed an in situ probe (LDHs-DGT) based on the diffusive gradients in thin-films technique using a single binding layer to realize the co-measurement of multi-elements including sulfide and oxyanions. Mg–Al layered double hydroxides (LDHs) were synthesized and incorporated into the probe's binding layer. Laboratorial characterization showed that the LDHs-DGT probe had a high capacity for sulfide, phosphate and arsenate and can effectively determine their levels across a wide range of solution conditions, i.e., pH from 5 to 8 and ionic strengths from 0.005–0.01 mol L<sup>−1</sup> NaNO<sub>3</sub>. The application potential of the LDH<sub>5</sub>-DGT probe in capturing the concentration profiles of sulfide and oxyanions across the soil/sediment–water interface at a centimeter scale was demonstrated. The synchronous co-variations of labile sulfide and phosphate were observed along an intact river sediment core, demonstrating the redox driven behaviors of oxyanions at aerobic–anaerobic transition zones. Moreover, the LDH<sub>5</sub>-DGT probe was further used to acquire the dynamic distributions of multi-elements in the plant rhizosphere at a two-dimensional millimeter scale. Compared to treatments of sodium sulfate and mercaptopygorskite fertilization, the addition of elementary S promoted the reduction of sulfate to sulfide along the whole growth stage and thus inhibited the activation of toxic metals in the rice rhizosphere. Collectively, this study provides a tool for convenient measurement of nutrients and metal(loid)s across soil–water/root interfaces at high resolution and thus, a broad application prospect of the tool in sustainable agriculture is expected.

**Keywords:** in situ sampling; nutrients; metal(loid)s; crop rhizosphere; sustainable agriculture

## 1. Introduction

For sustainable agriculture, it is important to keep the balance of mineral elements in soils, and to control the uptake and accumulation of toxic metal(loid)s in crops [1,2]. The biogeochemical cycling of mineral elements and toxic metal(loid)s in the environment is highly interlinked. For example, it has been found that sulfur (S) and phosphorus (P) affect the environmental behavior of arsenic (As) [1,3–5]. Under anoxic soil conditions, microorganisms promote the formation of sulfide and thus act as reducing agents for arsenic, promoting the release of As into the solution phase [6]. Alternatively, sulfide

may immobilize As by inducing co-precipitation of iron sulfide minerals (e.g., pyrite) and arsenic sulfide (dioecious and realgar) [6,7]. Phosphates and arsenates are considered chemical analogues, which means they can be substituted for each other in chemical reactions, including adsorption/desorption reaction, precipitation/dissolution reaction [4]. Besides, the distribution of elements in agricultural soils, especially at the crop rhizosphere, are highly uneven at both spatial and temporal scales. Therefore, it is strongly necessary to develop in situ high-resolution tools for co-measurement of nutrients and metal(loid)s at the soil/sediment–water interface and crop rhizosphere.

Diffusive gradients in thin films (DGT) is a representative in situ measurement technique characterized by broad applicability, quantitative measurement, trace element identification and high spatial resolution [8,9]. It is widely used for measurement of over 100 analytes including nutrients, metal(loid)s, radionuclides and polar organic contaminants in water, sediment and soil [8,10–15]. Typically, DGT is consistent of a protective filter membrane, a well-defined diffusion gel and a functionalized binding gel [16]. For the determination of different types of analytes, specific binding gels with incorporated binding materials are required [14,17]. Ideally, the binding gel should (1) have a high capacity for long-term monitoring of the target analytes; (2) contain particular binding materials with even distribution and small particle size for high-resolution application at interfaces [11,18]. The development of new bindings agents has received increasing attention in recent years. Specially, for the co-measurement of sulfide and oxyanions (e.g., phosphate and arsenate) using DGT two strategies are currently employed. One strategy involves the simultaneous application of two DGT probes with different binding layers that separately measure sulfide and oxyanions, e.g., AgI-DGT for sulfide, and ferrihydrite, Zr-oxide, or Metsorb-DGT for oxyanions [8,12,19,20]. The second strategy involves the application of a single type of DGT with a mixed binding layer, in which two kinds of functionalized materials such as AgI and ferrihydrite, AgI and Zr-oxide, or AgI and Metsorb were incorporated [16,20–23]. Although significant progress has been made in the development of binding gels, they often have some defects, such as poor mechanical resistance, poor repeatability or unclear gel structure which limit their application [2]. In this study, we propose a third strategy to achieve the co-measurement of sulfide and oxyanions based on DGT. In this new strategy, a DGT probe with a single functionalized material in the binding layer is sufficient. This is achieved by exploiting the ability of layered double hydroxides (LDHs) to capture different types of ions, including sulfide and oxyanions, thus overcoming the current limitations of binding gels.

LDHs are a type of anion adsorption material that is widely used in diverse industries for catalysis, adsorption and ion exchange, and are also used as functionalized environmental materials [24]. LDHs are layered compounds that aggregate the positively charged main laminate and the interlaminar anions. Because the interlayer anions in LDHs can be replaced by other anions, the target anions are thus immobilized in the interlayer [24,25]. However, there are significant differences in the anion exchange rates for different types of LDHs. Mg-Al LDHs synthesized from the chloride salts of magnesium and aluminum show excellent sorption capacity towards sulfide and oxyanions (e.g., P and As), while the incorporated Cl<sup>-</sup> helps reduce interference caused by other anions, e.g., nitrate [15,26,27]. In this study, Mg-Al LDHs nanoparticles were synthesized and used for as a single binding material in the LDHs-DGT probe. We hypothesized that the Mg-Al LDH<sub>5</sub> nanocomposite binding could adsorb both sulfide and oxyanions. The objective of this study is to (1) construct an in situ probe and characterize its performance for accurate measurement of labile concentrations of multi-elements in waters; (2) demonstrate the application potential of the probe in high-resolution measurement of nutrients/metal(loid)s at the soil/sediment–water interface and rice rhizosphere. This study provides a useful tool for management of nutrients and metal(loid)s in sustainable agriculture.

## 2. Materials and Methods

### 2.1. Reagents, Materials, and Solutions

The glassware and plastic materials used for probe construction were rinsed with 10% HNO<sub>3</sub> followed by rinsing with ultra-pure water (18.2 Ω cm, Milli-Q, Millipore, USA) three times before use to avoid sample contamination. All the solutions were prepared using ultra-pure water and all reagents used were of reagent-grade purity. Stock solutions (1 g·L<sup>-1</sup>) were prepared using KH<sub>2</sub>PO<sub>4</sub>, Na<sub>2</sub>S, Na<sub>2</sub>SO<sub>4</sub>, Na<sub>2</sub>HAsO<sub>4</sub>·7H<sub>2</sub>O and NaAsO<sub>2</sub>. MgCl<sub>2</sub>·6H<sub>2</sub>O, AlCl<sub>3</sub>·6H<sub>2</sub>O, NH<sub>4</sub>·OH, Diethylenetriaminepentaacetic acid (DTPA) were used to make LDH<sub>5</sub> nanoparticles.

### 2.2. Laboratory Evaluation of DGT Performance

#### 2.2.1. Synthesis and Characterization of LDHs

The LDHs were synthesized in accordance with a Chinese patented method [15]. An aqueous solution of magnesium chloride and aluminum chloride was prepared with a Mg<sup>2+</sup> (0.5 mol L<sup>-1</sup>):Al<sup>3+</sup> (0.5 mol L<sup>-1</sup>) ratio of 2:1 (in order to fully exchange anions in the solution to be tested), 0.5 mol L<sup>-1</sup> DTPA was then added to the solution. The milli-Q water configuration was used for all solutions. Under a stirring frequency of 40–50 Hz/s, 20–25% ammonia solution was slowly added when necessary to keep the pH of the reaction solution between 9.5. The mixture was continuously stirred for 30 min, and the aging reaction was allowed to occur for 60–120 min (25 °C). To make the precipitation reaction complete, ultra-pure water was then continuously added to the reaction mixture. The resulting LDHs precipitate was cleaned using ultra-pure water to remove chloride ions. After being stored overnight at –60 °C in an ultra-low temperature freezer (ZX-LGJ-18A, Zhixin, CHN), the precipitate was finally freeze-dried to obtain the requisite Mg–Al LDHs nanomaterials.

The crystal phases of the LDHs samples were examined by X-ray powder diffraction (XRD, D/MAX2500, Rigaku Corporation, JPN). The size and morphology of the samples were characterized by field emission scanning electron microscopy (FESEM, LEO 1350VP, LEO Electron Microscopy Ltd., GER) and transmission electron microscopy (TEM, JEM 2010, JEOL Ltd., JPN).

#### 2.2.2. Probe Gel Preparation

LDH<sub>5</sub> gel strips (0.6 mm thickness, ~10 cm × 17 cm) were made according to an established procedure [15]. To synthesize the binding gel, LDHs nanomaterials (2 g) were subjected to ultrasonication for 2–3 min [28]. Thereafter, tetramethylethylenediamine (TEMED) catalyst (22.5 μL) and freshly prepared ammonium persulfate initiator (90 μL, 10% w/v) were added. After sufficient stirring, the mixture was immediately cast between two glass plates separated by plastic spacers (ensuring that the LDH<sub>5</sub> gel thickness is 0.6 mm) and allowed to set at 42 °C for 1 h. Thereafter, the gel obtained was removed and placed in ultra-pure water, which was changed frequently within 24 h to remove the interference of nitrate ions. The diffusion gel was cross-linked with 15% acrylamide and 0.3% agarose derivatives according to an established procedure [12]. The diffusive gel and the binding gel were cut with a ceramic knife and assembled into DGT probes (Figure S1), which were then placed in a sealed pocket containing 0.01 M NaCl protective solution and stored in a refrigerator at 4 °C [15]. The gel strips were cut into circular discs (1 cm diameter) for use in LDH<sub>5</sub>-DGT characterization experiments (Figure S2). For LDH<sub>5</sub>-DGT deployment across the soil/sediment–water interface and rice rhizosphere, the gel strips were firstly cut into a size of 2.5 cm × 15 cm and 9 cm × 12 cm, respectively.

#### 2.2.3. Chemical Analysis and Concentration Calculation

To avoid oxidation of S(II) and As(III), experiments were carried out under nitrogen. The solution temperature was monitored during probe deployment. Upon retrieval, the probes were rinsed with ultra-pure water and the binding gel was then eluted with HNO<sub>3</sub> (9 mL, 0.5 mol·L<sup>-1</sup>) for 10 min. The concentrations of sulfur, phosphorus and ar-

senic in the LDH<sub>5</sub>-DGT eluates and solutions were determined via inductively coupled plasma mass spectrometry (ICP-MS, 7700×, Agilent, USA), high-performance liquid chromatography (HPLC, 1100, Agilent), and ion chromatography (IC, ICS3000, DIONEX, USA) calibrated using standard solutions of S(-II), phosphate (P), As(III) and As(V) and SO<sub>4</sub><sup>2-</sup>. DGT measured concentrations were calculated based on Fick's first diffusion law [8]:

$$M = \frac{C_e (V_g + V_e)}{f_e} \quad (1)$$

$$C_{DGT} = \frac{M \Delta g}{DA t} \quad (2)$$

where  $M$  represents the mass of the analyte bound onto the gel (ng),  $C_e$  represents the concentration of the analyte in the eluent ( $\mu\text{g L}^{-1}$ ),  $V_g$  represents the volume of the gel,  $V_e$  represents the eluent volume (mL), and  $f_e$  represents the elution efficiency ( $100 \pm 5\%$  for LDHs, which can be approximated as 1).  $\Delta g$  represents the sum of the thicknesses of the diffusive gel and the nitrocellulose film (0.089 cm),  $D$  represents the diffusion coefficient of the target analyte in the diffusive gel ( $\text{cm}^2 \text{s}^{-1}$ ),  $A$  represents the area of the DGT window ( $3.15 \text{ cm}^2$ ), and  $t$  represents the DGT deployment time (86,400 s).

#### 2.2.4. Diffusion Coefficients in the Probe's Diffusive Layer

The diffusion coefficient of each analyte in the diffusion gel was measured using the probe time-series deployment method [29]. Triplicate LDHs-DGT probes were placed in a solution containing S(-II), SO<sub>4</sub><sup>2-</sup>, phosphate, As(V), or As(III) (3.5 L, pH =  $5.5 \pm 0.2$ ) at  $25.0 \pm 0.5 \text{ }^\circ\text{C}$ , with an ionic strength of 0.01 M NaNO<sub>3</sub>. The concentration of each ion in the test solution was approximately  $700 \mu\text{g L}^{-1}$ . LDH<sub>5</sub>-DGT probes were retrieved after 2, 4, 6, 8, 10, 14 or 15 h, and the binding gels were taken out for analysis. An aliquot of the solution (2 mL) was collected each time and filtered ( $0.45 \mu\text{m}$ ) for analysis. The effective diffusion coefficients of S(-II), SO<sub>4</sub><sup>2-</sup>, phosphate, As(III) and As(V) were calculated using Equation (3) [12,29].

$$D = \frac{\text{slope} \times \Delta g}{c_{sol} \times A \times 60} \quad (3)$$

where "slope" refers to the linear regression slope of the mass (ng) of the ions accumulated in the gel with time (min); " $c_{sol}$ " is the concentration of the substance to be measured in the preparation solution ( $\mu\text{g L}^{-1}$ ).

#### 2.2.5. Selectivity of LDHs-DGT Probe to Sulfide and Arsenate

To determine the selectivity of the probe toward different forms of S (i.e., S(-II) and SO<sub>4</sub><sup>2-</sup>) and As (i.e., As(V) and As(III)), the LDHs-DGT probes were deployed in a mixed solution (3 L) containing S(-II) and SO<sub>4</sub><sup>2-</sup>, both at a concentration of  $50 \mu\text{g L}^{-1}$ . A similar experiment was conducted for As(III) and As(V), with both being at a concentration of  $50 \mu\text{g L}^{-1}$ . The solution was stirred thoroughly, and the LDH<sub>5</sub>-DGT probe was retrieved at 2, 4, 6, 8, 12, 24, 48 and 72 h, and at each time point, aliquots (10 mL) of the solution were collected to determine the concentrations of the chemical species. The concentrations of S(-II) were determined via ICP-MS, whereas SO<sub>4</sub><sup>2-</sup> was quantified by IC and As(III) and As(V) via HPLC-ICP-MS [30–32].

#### 2.2.6. Effects of Ionic Strength and pH on Probe Measurement

To study the effect of pH on probe measurement, the LDHs-DGT probe was immersed in a multi-element solution containing three different ions (phosphate, S(-II) and As(V)) at a concentration of approximately  $50 \mu\text{g L}^{-1}$  (KH<sub>2</sub>PO<sub>4</sub>, Na<sub>2</sub>S, Na<sub>2</sub>HAsO<sub>4</sub>). HNO<sub>3</sub> and NaOH were used to adjust the solution pH in the range 4–9. The LDHs-DGT probe was deployed in the solution for 6 h. To test the performance of the probe under different ionic strengths, the LDH<sub>5</sub>-DGT probe was exposed to a multi-element solution containing three ions (S(-II), phosphate and As(V)) at a concentration of approximately  $50 \mu\text{g L}^{-1}$  for 6 h.

The ionic strength in the solution was varied in the range 0.001–0.7 mol L<sup>-1</sup> NaNO<sub>3</sub>. The concentrations of phosphate, S(-II) and As(V) in the solutions and eluents of binding gel were analyzed.

### 2.2.7. Capacity of the Probe

To determine the capacity of the probe with respect to the S(-II), phosphate and As(V) ions, the LDH<sub>5</sub>-DGT probe was immersed in a 1 L well-stirred solution with a single solution of 0.5–120 mg L<sup>-1</sup> for 24 h. Before the deployment of the LDH<sub>5</sub>-DGT probe, the test solution was stirred vigorously for three days, while ensuring that a constant solution pH at 5.5 using dilute solutions of HNO<sub>3</sub> and NaOH. After deployment of the LDH<sub>5</sub>-DGT probes, DGT-measured S(-II), phosphate and As(V) concentrations were determined via ICP-MS and the capacity of the LDH<sub>5</sub>-DGT probe thus obtained through comparison with the theoretical uptake concentrations.

### 2.2.8. Competition Effect among Different Elements

To test the possible interference of several kinds of ions on DGT measurement, the LDH<sub>5</sub>-DGT probe was deployed in a mixed solution (2 L) containing S(-II), phosphate and As(V). The ion concentration of the mixed solution was in the range of 4–90 µg L<sup>-1</sup> at pH 5.5. The highest ion concentration of 90 µg L<sup>-1</sup> was 9-fold to that of P and 1.8-fold to those of As and S, based on the Chinese Surface Water Environmental Quality Standard [33]. The probe deployed in each solution was retrieved after 8 h, and the concentrations of the ions in the solutions and eluants were both determined.

### 2.3. Co-Measurement of Multi-Elements Using LDH<sub>5</sub>-DGT Probe in Water

Three water samples were collected from three different waterbodies (0–20 cm) in Tianjin, China. The first sample (“W1”) is agricultural irrigation water from Tianjin, which is used to represent the baseline concentration of S(-II), phosphate and As(V). The other two sites were from the Jinhe River (“W2”, represents high eutrophication levels) and the park fountain (“W3”, represents low eutrophication levels) with different levels of S(-II), phosphate and As(V). These samples demonstrate some extreme scenarios challenging LDH<sub>5</sub>-DGT measurements. After sampling, all water samples were filtered through a 0.45 µm membrane. A pH meter (S8-FEID Kit, Mettler Toledo, GER) was used to determine the sample pH. The S(-II) concentration was determined by methylene blue spectrophotometry [5], whereas the concentration of phosphate was directly determined by ICP-MS after HNO<sub>3</sub> acidification and that of As(V) was determined by HPLC-ICP-MS. Triplicate LDH<sub>5</sub>-DGT probes were deployed in the water sample (2 L) at 25 ± 1 °C [34]. The probes were retrieved after 24 h, rinsed with ultra-pure water. The binding gel was removed and eluted with 9 mL 0.5 mol L<sup>-1</sup> HNO<sub>3</sub> eluent. The concentrations S(-II), phosphate and As(V) were determined in the eluants were then measured.

### 2.4. High-Resolution Measurement of Multi-Element Distribution at Soil/Sediment-Water Interface

To test the applicability of the LDH<sub>5</sub>-DGT probe for high resolution measurement across the soil/sediment–water interface, an intact sediment core with overlying water was collected from the eutrophic Jinhe River in Tianjin, China in July 2020. Three deoxygenated LDH<sub>5</sub>-DGT probes were inserted into the core for 48 h, and after retrieval, the binding gel was cut into 1 cm-long fragments. Each fragment was eluted with HNO<sub>3</sub> (9 mL, 0.5 mol L<sup>-1</sup>), and the concentrations of S(-II), phosphate and As(V) were determined via ICP-MS and calculated according to Equation (2). By assigning DGT-measured concentrations to the ordinated vertical location information, 1D concentration profile of the three ions across the interface was obtained [35].

### 2.5. Application of LDHs-DGT Probe in Rice Rhizosphere for Imaging of the Dynamic Distributions of Multi-Elements

In order to study the spatial and temporal dynamic distribution characteristics of different forms of exogenous sulfur on S(-II) and toxic metals (e.g., Cd) in rice rhizosphere soil, a rhizo-box was built for efficient LDHs-DGT probe deployment. It can provide the technical means and theoretical basis for studying the temporal and spatial dynamic characteristics of S(-II) and the biogeochemical cycle of S(-II) and other elements in paddy fields. A paddy soil contaminated with toxic metal(loid)s including Cd was collected from Hunan, China and used for the rhizo-box experiment, which was carried out from April to October 2020. About 1.5 kg soil (dry weight) was filled into each rhizo-box with length  $\times$  width  $\times$  height of 15 cm  $\times$  5 cm  $\times$  25 cm. There were 4 treatments: A-control (CK), B-elementary S<sup>0</sup> (S<sup>0</sup>: 100 mg/kg), C-sodium sulfate (Na<sub>2</sub>SO<sub>4</sub>: 100 mg/kg) and D-mercaptopygoroskite (MP: 100 mg/kg), and each treatment has three replicates. Nutrients (N: urea 1.50 g/kg; P, K: potassium dihydrogen phosphate 1.10 g/kg) were mixed evenly with the soil samples and the overall soil layer was maintained with a same height. Then, a foil paper was placed around the transparent glass plate to protect it from light. Finally, deionized water was added to maintain a constant 2-cm flooded layer for 4 weeks.

The experimental setup is shown in Figures 1 and S3. Rice seedlings (Mingzhu silk-H variety) with 3 leaves were transplanted in the rhizo-box, which was then maintained at a 70° inclination to facilitate root growth along the lower front window (to ensure that rice roots grow along the glass plate). At rice growing stages of tillering, heading, maturing, the detachable front glass plate was removed, and the LDHs-DGT probe binding gel was placed at the rhizosphere zone and kept in close contact with the PVDF membrane (thickness of 100  $\mu$ m and pore size of 0.45  $\mu$ m). After overlying the gel with a nitrocellulose membrane protective filter, the removed glass plate was installed back. The probe gel was retrieved from the rhizo-box after deployment for four days. Afterwards, photos of the distribution of root system were taken using a digital camera. The distribution of S(-II) and a common toxic metal, Cd, in the gel was analyzed using ICP-MS. 2D images of S(-II) and Cd at rice rhizosphere were acquired after calculation using equation 2 and position assignment to the ordinated rhizosphere environment.

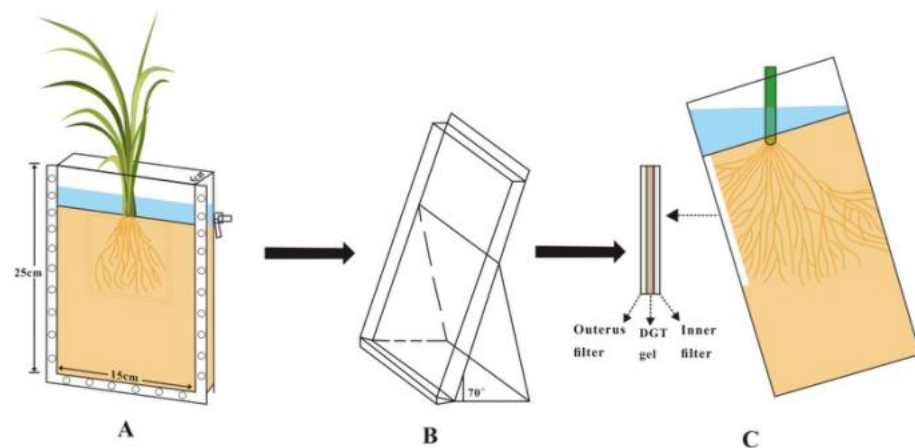


**Figure 1.** Experimental setup for imaging of the dynamic distributions of multi-elements in rice rhizosphere using LDHs-DGT probe. (A) The dimensions and arrangement of the rhizotron; (B) the rhizotron was tilted to an angle of 70° throughout the whole experiment; (C) cross-section showing the deployment sequence of inner filter. Modified from He [36].

## 3. Results and Discussion

### 3.1. Laboratorial Characterization of the Performance of the LDHs-DGT Probe

#### 3.1.1. Morphology and Structural Characterization of LDH<sub>5</sub>

The morphology and particle size of the synthesized LDH<sub>5</sub> were identified by FESEM and TEM. The FESEM micrographs in Figure S4A show that the LDHs exhibited a plate-

like morphology, which is typical for layered double hydroxides, and the platelet size was approximately 200 nm. TEM characterization confirmed the hexagonal shape of the particles (Figure S4B). The existence of LDHs was confirmed by the X-ray diffraction pattern (Figure S4C), in which the major diffraction peaks matched well with the simulated pattern of LDH<sub>5</sub>. The d-spacing of LDH<sub>5</sub> samples was approximately 1.42 nm, and the channel height was approximately 0.94 nm. This result indicates that LDHs exist at an angle relative to the brucite layers. The molecular structure of the LDH<sub>5</sub> is shown in Figure S4D.

### 3.1.2. Diffusion Coefficient of Multi-Elements in LDH<sub>5</sub>-DGT Diffusive Layer

The diffusion coefficients of phosphate, SO<sub>4</sub><sup>2-</sup>, S(-II), As(III) and As(V) were determined by the DGT time-series deployment method [19,37]. Linear relationships were also observed for the accumulated mass of phosphate, SO<sub>4</sub><sup>2-</sup>, S(-II), As(III), and As(V) with their concentrations (Figure S5). The diffusion coefficients of S(II), SO<sub>4</sub><sup>2-</sup>, phosphate, As(III) and As(V) at 25 °C (Table 1) in the LDH<sub>5</sub>-DGT diffusion gel were in the order of 10<sup>-6</sup> [24,38], but were somewhat lower than those of the APA gel and the agarose gel. This is because the diffusion gel of LDH<sub>5</sub>-DGT is made of acrylamide, which has a small pore size (<5 nm). However, the APA and agarose gels had larger pore sizes of >5 nm and >20 nm, respectively [34]. A larger pore size will produce a lower tortuosity within the gel and promote ion diffusion [34]. Additionally, APA and agarose gels have a small positive charge, and thus, Donnan partitioning at the gel–solution interface is possible, thereby increasing the diffusion coefficients of the anionic species [39].

**Table 1.** Diffusion coefficient (E<sup>-6</sup> cm<sup>2</sup> s<sup>-1</sup>) measured by LDH<sub>5</sub>-DGT devices at 25 °C. Data are mean ± SD (*n* = 3).

Analyte	S(-II)	SO <sub>4</sub> (II)	Phosphate	As(III)	As(V)
D <sub>DGT</sub>	5.99 ± 0.12	7.50 ± 0.28	4.57 ± 0.14	3.73 ± 0.15	3.41 ± 0.10

### 3.1.3. Selectivity of LDH<sub>5</sub>-DGT Probe for Sulfide and Arsenate

Realizing the in situ measurement of S(-II) and As(V) is important in determining the selectivity of the LDH<sub>5</sub>-DGT probe. The amount of As(V) captured by LDH<sub>5</sub>-DGT from the mixed solution increased linearly with time, while the amount of retained As(III) was below 4% even after 72 h (Figure S6). Similarly, when SO<sub>4</sub><sup>2-</sup> and S(-II) ions co-existed in the solution, the mass of S(-II) by LDH<sub>5</sub>-DGT increased linearly with time as expected, but the capture of SO<sub>4</sub><sup>2-</sup> was highly inefficient, i.e., below 4% after 72 h (Figure S6). Therefore, LDH<sub>5</sub>-DGT can achieve in situ selective adsorption of S(-II) and As(V).

### 3.1.4. Effects of pH and Ionic Strength on the Measurement of LDH<sub>5</sub>-DGT Probe

The effects of environmental conditions on the performance of the LDH<sub>5</sub>-DGT were investigated by deploying the LDH<sub>5</sub>-DGT in a mixed solution containing phosphate, S(-II), and As(V) under different pH conditions (pH 4–9) and ionic strengths (0.001–0.7 mol L<sup>-1</sup> NaNO<sub>3</sub>) (Figure 2). The ratio of DGT-measured concentrations to those in solutions (C<sub>DGT</sub>/C<sub>sol</sub>) is widely used to judge the performance of the DGT probe and 0.9–1.1 indicates a good performance [12]. In the solution with pH in the range of 5–8, the ratios were all in the range of 0.9–1.1. However, at pH < 5 or pH > 8, the ratio was below 0.9. This can be explained by that the presence of excess hydrogen ions at pH < 5 that inhibit the adsorption of the analytes onto the binding gel [12,28]. Further, under low pH conditions, the LDHs structure is less stable, thereby reducing the adsorption of the analytes [40]. Furthermore, under higher pH conditions (pH > 8), the hydroxide precipitation that occurs on the surface of the LDH<sub>5</sub> may affect the gel's adsorption performance [40]. LDH<sub>5</sub>-DGT performed well when ionic strength was at 5–100 mmol L<sup>-1</sup> NaNO<sub>3</sub> (Figure 2B). The ratio of C<sub>DGT</sub> to C<sub>sol</sub> decreases with an increase in ionic strength due to the fact that the ionic strength of the solution affects the activity coefficient of the ions [40]. At extremely low ionic strength (1 mmol L<sup>-1</sup> NaNO<sub>3</sub>), the ratio for S(-II) and As(V) was slightly higher than

1.1. This is probably caused by the formation of an electric double layer complex within the LDHs materials which improves adsorption [24] or electrostatic interactions due to particle aggregation in LDHs [41]. At high ionic strength ( $700 \text{ mmol L}^{-1} \text{ NaNO}_3$ ), the solvation shell around the ions becomes larger and the activity coefficient increases [40], causing a lower ratio than 0.9. Therefore, the LDHs-DGT is suitable for measuring multi-elements at pH of 4–8 and ionic strength at 5–100  $\text{mmol L}^{-1} \text{ NaNO}_3$ . For sole measurement of phosphate using LDHs-DGT, the environmental conditions can be slightly extended.

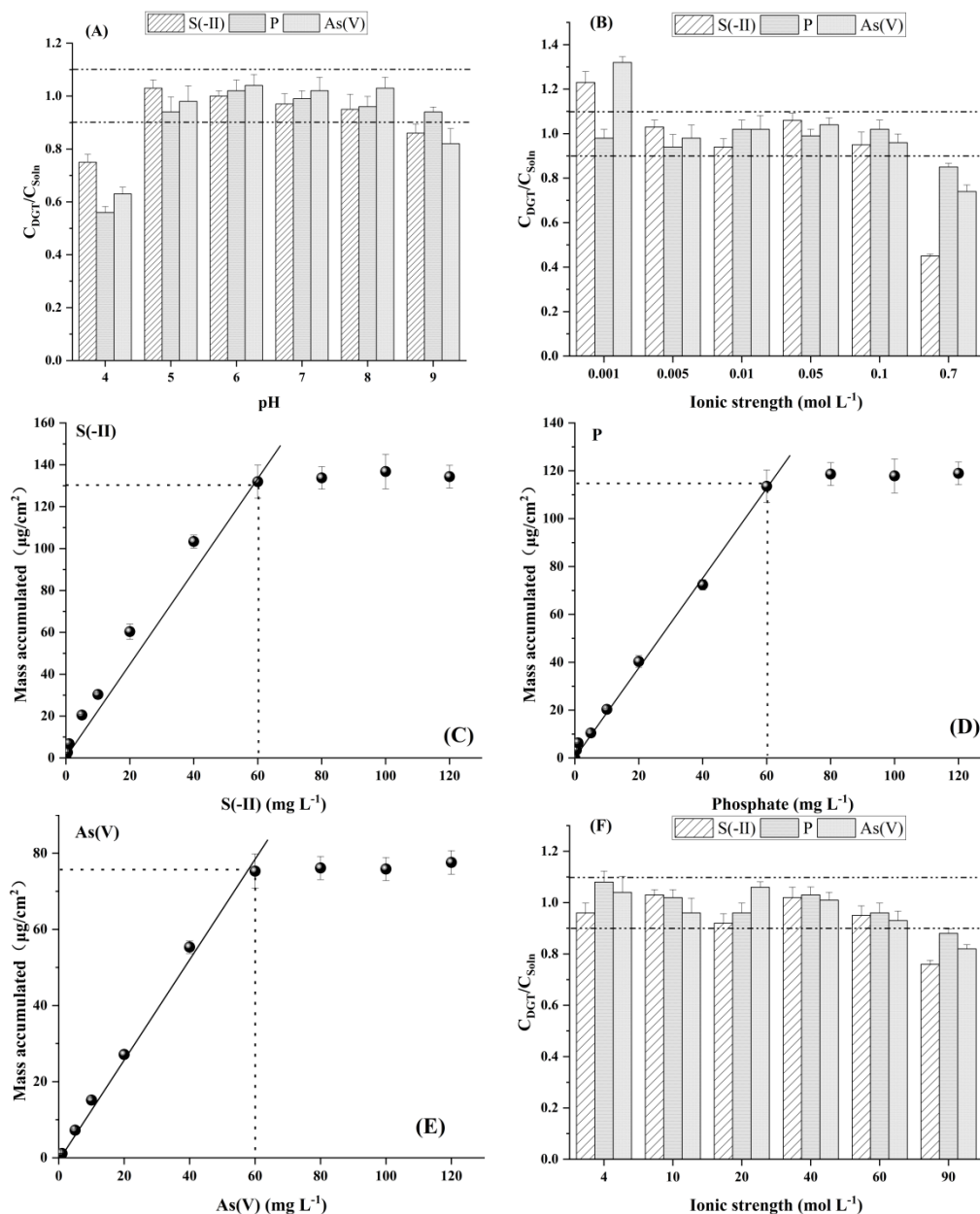


**Figure 2.** Effect of pH (A) and ionic strength (B) on measurement of S(-II), P and As(V) by LDH<sub>5</sub>-DGT, time-dependent mass accumulation of S(-II) (C), P (D) and As(V) onto LDH<sub>5</sub>-DGT binding gel, and competition effect among S(-II), P and As(V) for their LDH<sub>5</sub>-DGT measurement (F). In (A,B), the solutions contained  $50 \mu\text{g L}^{-1}$  mixed ions of S(-II), P and As(V). The data are presented as average  $\pm$  standard deviations ( $n = 3$ ). The lower and higher dotted lines in (A,B,F) represent the values of 0.9 and 1.1, respectively, whereas the dotted lines in (C-E) indicate the capacity for S(-II), P and As(V) measured by LDH<sub>5</sub>-DGT.

### 3.1.5. Capacity of LDH<sub>5</sub>-DGT Probe for Measurement of Sulfide, Phosphate and Arsenate and Their Competition Effects

The capacity of LDH<sub>5</sub>-DGT was investigated by deploying the probes in solutions containing S(-II), phosphate and As(V) with concentrations in the ranges ~0.5–120 mg L<sup>-1</sup> (pH = 5.50, IS = 0.01 mol L<sup>-1</sup> NaNO<sub>3</sub>). The mass of the ions measured in the LDH<sub>5</sub>-DGT binding gel increased linearly with their concentration in the solution (Figure 2C–E) until the capacity was reached. Specifically, the capacities for S(-II), phosphate and As(V) were as high as 131.98, 113.56 and 75.31 µg cm<sup>2</sup>, respectively. The capacity for S(-II) of LDH<sub>5</sub>-DGT, was slightly lower than those of AgI and ZrO-AgI [37,38], but the capacity of LDH<sub>5</sub>-DGT for phosphate was higher than those of Chelex-100 (102 µg cm<sup>2</sup>) and ZrO-Chelex (90 µg cm<sup>2</sup>). Even though the capacity of LDH<sub>5</sub>-DGT for As was lower than those of ZrO-Chelex and ZrO-CA (87.4 and 90.0 µg cm<sup>2</sup>, respectively), it was still much higher than those of precipitated zirconia, Metsorb, precipitated/slurry ferrihydrite, and ZrO-CA (s) (42.6, 26.1, 27.7/10 and 47.2 µg cm<sup>2</sup>, respectively) [18,29,42,43]. This is because LDHs have a large surface area and a flexible intermediate region, which enables them to absorb large amounts of oxyanions [24]. Therefore, LDH<sub>5</sub>-DGT has a high capacity for multi-elements and is suitable for long-term deployment in diverse environments.

The possible competition effect among the tested analytes was investigated and the results are shown in Figure 2F. When the ion concentration of the mixed solution was in the range of 4–60 µg L<sup>-1</sup>, the ratio ( $C_{DGT}/C_{soln}$ ) was within the expected range of values (0.9–1.1) indicating that there is no significant competition between unstable species at the binding sites [19]. Only a slight competition effect was observed at high ion concentration at 90 µg L<sup>-1</sup>. Generally, for LDH<sub>5</sub>-DGT, the competition effect among ions was negligible.

### 3.2. Measurement of Labile Concentrations of Multi-Elements in Field Waters Using LDH<sub>5</sub>-DGT Probe

The chemistries and hydrological conditions of the water body affect the mobility and species of redox sensitive elements, and thus affect the water quality [44,45]. The concentrations of S(-II), phosphate and As(V) in sample W1 were 15.50, 24.62 and 8.53 µg L<sup>-1</sup>, respectively (Table 2), which represent the characteristics of a common water body. Among them, the concentration of phosphate exceeds the pollution threshold for surface water (0.02 mg L<sup>-1</sup>) [46]. The concentration of phosphate in sample W2, representing an eutrophicated water body, is 74.52 µg L<sup>-1</sup>, which is 3.8 times higher than the threshold. The concentration of S(-II), phosphate and As(V) in sample W3, which was taken from an artificial lake, were 10.26, 19.45 and 12.22 µg L<sup>-1</sup>, respectively, which indicates that the surface water is uncontaminated. This study is the first time that the LDH<sub>5</sub>-DGT technique has been applied in the simultaneous determination of S(-II), phosphate and As(V) levels in water. The R value (ratio of  $C_{DGT}$  to  $C_{sol}$ ) at the range of 0.9–1.1 (Table 2) reflects the reliability of LDH<sub>5</sub>-DGT measurement in real water samples.

**Table 2.** The pH of the water samples, concentrations of S(-II), phosphate, and As(V) in water ( $C_{water}$ ) and those measured by LDH<sub>5</sub>-DGT ( $C_{DGT}$ ), and the ratios (R) of  $C_{water}/C_{DGT}$ . Data are mean ± SD ( $n = 3$ ).

Water	W1	W2	W3
pH	6.81 ± 0.07	5.93 ± 0.06	7.26 ± 0.07
S(-II)- $C_{water}$ (µg L <sup>-1</sup> )	15.50 ± 0.62	58.46 ± 4.09	10.26 ± 0.51
Phosphate- $C_{water}$ (µg L <sup>-1</sup> )	24.62 ± 0.49	74.52 ± 2.24	19.45 ± 0.58
As(V)- $C_{water}$ (µg L <sup>-1</sup> )	8.53 ± 0.17	4.34 ± 0.09	12.22 ± 0.49
S(-II)- $C_{DGT}$ (µg L <sup>-1</sup> )	14.11 ± 0.42	54.92 ± 1.65	9.23 ± 0.28
Phosphate- $C_{DGT}$ (µg L <sup>-1</sup> )	22.90 ± 0.69	72.28 ± 2.89	17.89 ± 0.54

Table 2. Cont.

Water	W1	W2	W3
As(V)-C <sub>DGT</sub> ( $\mu\text{g L}^{-1}$ )	8.10 $\pm$ 0.32	4.04 $\pm$ 0.08	11.36 $\pm$ 0.34
<sup>a</sup> R <sub>S(-II)</sub>	0.91	0.94	0.90
<sup>a</sup> R <sub>phosphate</sub>	0.93	0.97	0.92
<sup>a</sup> R <sub>As(V)</sub>	0.95	0.94	0.90

<sup>a</sup> Obtained by averaging the ratios of C<sub>DGT</sub> divided by C<sub>water</sub>.

### 3.3. Application of LDHs-DGT Probe in Soil/Sediment-Water Interface for Measurement of Multi-Elements at 1D Centimeter Scale

The vertical distributions of S(-II), phosphate and As(V) in sediments were measured using the LDH<sub>5</sub>-DGT (Figure 3). The average DGT concentrations of S(-II) and phosphate were higher in the vertical direction (51 and 56.3  $\mu\text{g L}^{-1}$ ), and the average DGT concentration of As(V) (5  $\mu\text{g L}^{-1}$ ) was significantly lower than those of phosphate and S(-II) ( $p < 0.05$ ). Additionally, the changes in the vertical concentrations of S(-II), phosphate and As(V) were larger, and that of S(-II) was largest. This confirms that the redox reaction, which mainly involves Fe and Mn cycling, is the main factor leading to the heterogeneity of the chemical distribution [34].

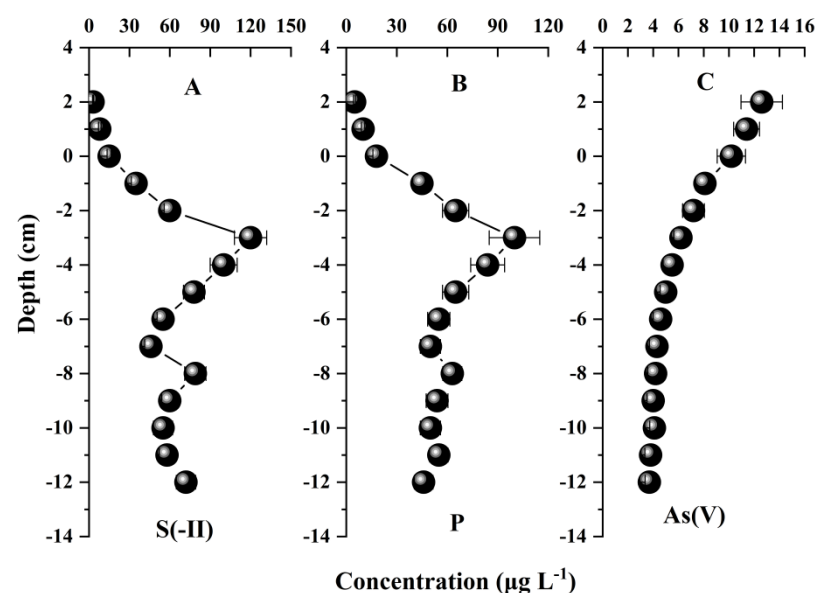


**Figure 3.** Vertical distributions of labile concentrations of S(-II) (A), phosphate (B) and As(V) (C) across sediment–water interface. The sediment core was collected from Jinhe River, Tianjin, China. Data were presented as the average values and standard deviations ( $n = 3$ ). The resolution of the concentration profile is 1 cm.

Even though the chemical distribution was uneven in the vertical direction, the vertical distributions of S(-II), phosphate and As(V) were similar. Their concentration increased rapidly from the overlying water to a maximum value at a depth of approximately 3 cm below the sediment–water interface. However, the concentration of S(-II) first decreased to a depth of 8 cm below the interface, then increased, and then decreased again; the concentration of phosphate decreased rapidly, and then stabilized to the bottom of the profile, whereas the concentration of As(V) dropped directly to the bottom of the profile. The unstable changes in the concentrations of S(-II), phosphate and As(V) in the DGT further demonstrate that they are released during the reductive dissolution of Fe and Mn oxides [25,44,47]. This generally shows that LDH<sub>5</sub>-DGT is highly useful for acquiring centimeter scale resolution concentration profiles of multi-elements and this function can be further played for exploring the processes in the soil–water interfaces.

### 3.4. Measurement of the Dynamic Distribution of Multi-Elements at Rice Rhizosphere at 2D Millimeter Scale

Imaging of element distribution at the rice rhizosphere tells previously hardly reached information at microniches. The images of S(-II) and Cd at three typical stages of rice growth are shown in Figures 4 and S7, with the resolution being at a millimeter scale (the data were interpolated to some extent). The uneven and dynamic distributions of the two elements were clearly shown. This highlights the necessity of 2D high spatio-resolution measurements.

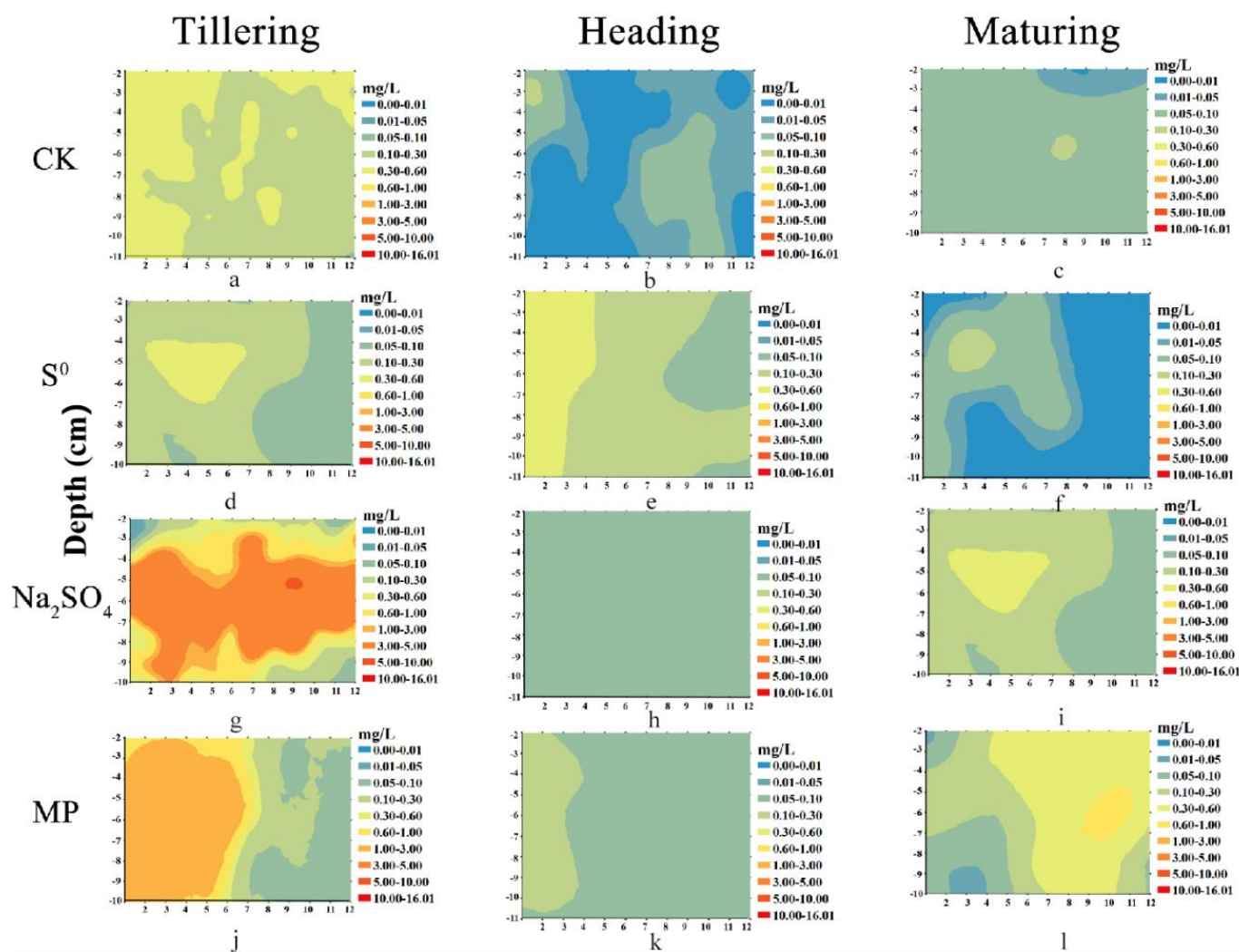


**Figure 4.** Two-dimensional distribution of S(-II) in the rhizosphere of rice at different growth stages (Tillering: a,d,g,j; Heading: b,e,h,k; Maturing: c,f,i,l). MP refers to mercaptopygorskite. Arc GIS 10.8 software was used to draw this figure.

The application of sulfur promoted the increase of S(-II) in rice root zone soil (Figure 4). This is mainly because flooding conditions can promote the increase of sulfate reducing bacteria and enhance sulfate reduction [48,49], thus promoting the increase of S(-II). In order to adapt to long-term flooding conditions, rice roots transport oxygen from above-ground leaves to the root system, and the root system secretes oxygen to the surrounding environment [50,51]. Therefore, the concentration of S(-II) in rhizosphere soil increased firstly, then decreased and then increased in different growth stages of rice. At heading stage, due to the formation of rhizome nodes, the process of oxygen transport from the ground to the root system is blocked [50]. In addition, S(-II) and Fe will form FeS precipitation [50], so the concentration of S(-II) in rhizosphere soil is the lowest. Thus, the formation of CdS is reduced, and Cd has the highest activity.

Sulfate reduction is an important process in controlling the dynamics of toxic metal(loid)s (e.g., Cd) in paddy soils [36,52,53]. The experimental results showed that the addition of S promoted the reduction of sulfate and inhibited the activation of Cd (Figures 4 and S4). Sulfate reduction can promote the formation of organic bound Cd and residual Cd, thus reducing labile Cd [15]. Therefore, the activity of Cd increased first and then decreased during the growth period of rice (Figure S4). Different S treatment groups resulted in distinct sulfuric acid reduction degree. Na<sub>2</sub>SO<sub>4</sub> had a stronger effect than that of mercaptopygorskite, and that of S<sup>0</sup> is the lowest, which highlights the importance of valence state of S. The results show that LDH<sub>5</sub>-DGT is able to capture the dynamic processes of multi-elements in the rice rhizosphere at a millimeter-scale high spatio-resolution. Further, LDH<sub>5</sub>-DGT can be combined with other imaging tools such as planar optode for pH and O<sub>2</sub> and soil zymography for enzyme activities to provide a holistic understanding of the highly complex processes in crop rhizosphere.

#### 4. Conclusions

This work provides a useful tool based on DGT technique for co-measurement of multi-elements, i.e., sulfides (S(-II)) and oxyanions (phosphate, As(V)). This is realized by taking advantage of the superior ion exchange properties of Mg-Al LDHs, which were used to prepare a novel binding gel in the LDH<sub>5</sub>-DGT probe. LDH<sub>5</sub>-DGT can be applied in a wide range of pH and ionic strength conditions. LDH<sub>5</sub>-DGT is able to capture the dynamic processes of multi-elements at soil/sediment–water interfaces and rice rhizosphere at high spatio-resolution (centimeter to millimeter scale). The co-measurement of 1D/2D processes in heterogeneous soils can significantly improve our understanding of the micro-niche biogeochemistry of inter-linked elements (e.g., sulfides and oxyanions) and prompt the establishment of fine management measures in sustainable agriculture.

**Supplementary Materials:** The following are available online at <https://www.mdpi.com/article/10.3390/agronomy11122383/s1>, Figure S1: LDH<sub>5</sub>-DGT probe device, Figure S2: LDH<sub>5</sub>-DGT test stand, Figure S3: Experimental setup for imaging of the dynamic distributions of multi-elements in rice rhizosphere using LDHs-DGT probe, Figure S4: SEM (A) and TEM images (B) of LDHs samples; XRD patterns of the standard and as-prepared LDHs (C); Schematic representation of LDHs structure (D), Figure S5: The accumulated mass of S(-II) (A), SO<sub>4</sub><sup>2-</sup> (B), phosphate (C), As(III) (D), As(V) (E) in the binding gel with the time of LDHs-DGT deployment. Values are mean ± SD (*n* = 3), Figure S6: LDHs-DGT uptake curve in mixed solution of S(-II) and SO<sub>4</sub><sup>2-</sup> (A), and As(III) and As(V) (B). The value is the average ± SD (pH = 5.50, *n* = 3), Figure S7: Two-dimensional distribution of labile Cd concentrations in rhizosphere at different growth stages of rice. MP refers to mercaptopygorskite. Arc GIS 10.8 (Esri, USA) software was used to draw this figure.

**Author Contributions:** Data curation, formal analysis, investigation, methodology, writing—original draft, writing—review & editing, M.Z. and J.L.; investigation, resources, validation, C.Z., X.L. (Xuefeng Liang), Q.E. and R.L.; funding acquisition, methodology, project administration, supervision, writing—review & editing, Y.Z. and X.L. (Xiaowei Liu). All authors have read and agreed to the published version of the manuscript.

**Funding:** This research was funded by the National Key Research and Development Program of China (No. 2016YFD0800307-4, and No. 2016YFD0800301-01).

**Data Availability Statement:** Data sharing not applicable.

**Acknowledgments:** We would like to thank Xiangyan Wang for the sample collection and preparation.

**Conflicts of Interest:** The authors declare no conflict of interest.

#### References

1. Deng, X.Z.; Guang, H.D.; Weng, J.Z.; Ya, G.; Hong, B.J.; Wei, R.; Ying, J.; Dai, C.W. Remediation of arsenic-contaminated paddy soil: Effects of elemental sulfur and gypsum fertilizer application. *Ecotoxicol. Environ. Saf.* **2021**, *223*, 112606.
2. Qin, W.; Gu, Y.; Wang, G.; Wu, T.; Zhang, H.; Tang, X.; Zhang, Y.; Zhao, H. Zirconium metal organic frameworks-based DGT technique for in situ measurement of dissolved reactive phosphorus in waters. *Water Res.* **2018**, *147*, 223–232. [[CrossRef](#)]

3. Pi, K.; Wang, Y.; Xie, X.; Ma, T.; Su, C.; Liu, Y. Role of sulfur redox cycling on arsenic mobilization in aquifers of Datong Basin, northern China. *Appl. Geochem.* **2017**, *77*, 31–43. [[CrossRef](#)]
4. Strawn, D.G. Review of interactions between phosphorus and arsenic in soils from four case studies. *Geochem. Transactions* **2018**, *19*, 10. [[CrossRef](#)] [[PubMed](#)]
5. Silva, M.; Da, S.; Abate, G.; Masini, J. Spectrophotometric determination of acid volatile sulfide in river sediments by sequential injection analysis exploiting the methylene blue reaction. *Talanta* **2001**, *53*, 843–850. [[CrossRef](#)]
6. Kirk, M.F.; Roden, E.E.; Crossey, L.J.; Brealey, A.J.; Spilde, M.N. Experimental analysis of arsenic precipitation during microbial sulfate and iron reduction in model aquifer sediment reactors. *Geochim. Cosmochim. Acta* **2010**, *74*, 2538–2555. [[CrossRef](#)]
7. Kocar, B.; Borch, T.; Fendorf, S. Arsenic repartitioning during biogenic sulfidization and transformation of ferrihydrite. *Geochim. Cosmochim. Acta* **2010**, *74*, 980–994. [[CrossRef](#)]
8. Davlson, W.; Zhang, H. In situspeciation measurements of trace components in natural waters using thin-film gels. *Nature* **1994**, *367*, 546–548. [[CrossRef](#)]
9. Kreuzeder, A.; Santner, J.; Prohaska, T.; Wenzel, W.W. Gel for simultaneous chemical imaging of anionic and cationic solutes using diffusive gradients in thin films. *Anal. Chem.* **2013**, *85*, 12028–12036. [[CrossRef](#)]
10. Anonymous, J.; Broney, C. *Environmental Chemistry Study Findings on Environmental Chemistry Are Outlined in Reports from A; Stockdale and Colleagues: Atlanta, GA, USA, 2008*; p. 371.
11. Guan, D.X. Diffusive Gradients in Thin-Films (DGT): An Effective and Simple Tool for Assessing Contaminant Bioavailability in Waters, Soils and Sediments. *Encycl. Environ. Health* **2019**, *1025*, 111–124.
12. Zhang, H.; Davison, W. Performance characteristics of diffusion gradients in thin films for the in situ measurement of trace metals in aqueous solution. *Anal. Chem.* **1995**, *67*, 3391. [[CrossRef](#)]
13. Zhang, H.; Davison, W.; Knight, B.; McGrath, S. In situ measurements of solution concentrations and fluxes of trace metals in soils using DGT. *Environ. Sci. Technol.* **1998**, *32*, 704–710. [[CrossRef](#)]
14. Zhang, H.; Zhao, F.J.; Sun, B.; Davison, W.; McGrath, S.P. A new method to measure effective soil solution concentration predicts copper availability to plants. *Environ. Sci. Technol.* **2001**, *35*, 2602–2607. [[CrossRef](#)]
15. Zhao, M.; Qian, E.; Zhang, F.; Liu, R.; Liu, X.; Zhao, Y.; Liang, X. Spatiotemporal dynamics of labile Cd in soil during rice growth. *Sci. Total Environ.* **2020**, *738*, 139832. [[CrossRef](#)] [[PubMed](#)]
16. Luo, J.; Zhang, H.; Santner, J.; Davison, W. Performance characteristics of diffusive gradients in thin films equipped with a binding gel layer containing precipitated ferrihydrite for measuring arsenic (V), selenium (VI), vanadium (V), and antimony (V). *Anal. Chem.* **2010**, *82*, 8903–8909. [[CrossRef](#)] [[PubMed](#)]
17. Knutsson, J.; Rauch, S.; Morrison, G. Estimation of Measurement Uncertainties for the DGT Passive Sampler Used for Determination of Copper in Water. *Int. J. Anal. Chem.* **2014**, *389125*, 1–7. [[CrossRef](#)]
18. Guan, D.X.; Williams, P.N.; Luo, J.; Zheng, J.L.; Xu, H.C.; Cai, C.; Ma, L.Q. Novel precipitated zirconia-based DGT technique for high-resolution imaging of oxyanions in waters and sediments. *Environ. Sci. Technol.* **2015**, *49*, 3653–3661. [[CrossRef](#)]
19. Ding, S.; Xu, D.; Wang, Y.; Wang, Y.; Li, Y.; Gong, M.; Zhang, C. Simultaneous Measurements of Eight Oxyanions Using High-Capacity Diffusive Gradients in Thin Films (Zr-Oxide DGT) with a High-Efficiency Elution Procedure. *Environ. Sci. Technol.* **2016**, *50*, 7572–7580. [[CrossRef](#)]
20. Österlund, H.; Chlot, S.; Faarinen, M.; Widerlund, A.; Rodushkin, I.; Ingri, J.; Baxter, D.C. Simultaneous measurements of As, Mo, Sb, V and W using a ferrihydrite diffusive gradients in thin films (DGT) device. *Anal. Chim. Acta* **2010**, *682*, 59–65. [[CrossRef](#)]
21. Fan, X.; Ding, S.; Chen, M.; Gao, S.; Fu, Z.; Gong, M.; Tsang, D.; Wang, Y.; Zhang, C. Peak Chromium Pollution in Summer and Winter Caused by High Mobility of Chromium in Sediment of a Eutrophic Lake: In Situ Evidence from High Spatiotemporal Sampling. *Environ. Sci. Technol.* **2019**, *53*, 4755–4764. [[CrossRef](#)]
22. Fan, X.; Ding, S.; Chen, M.; Gao, S.; Fu, Z.; Gong, M.; Wang, Y.; Zhang, C. Mobility of chromium in sediments dominated by macrophytes and cyanobacteria in different zones of Lake Taihu. *Sci. Total Environ.* **2019**, *666*, 994–1002. [[CrossRef](#)] [[PubMed](#)]
23. Panther, J.G.; Stewart, R.R.; Teasdale, P.R.; Bennett, W.W.; Welsh, D.T.; Zhao, H. Titanium dioxide-based DGT for measuring dissolved As (V), V (V), Sb (V), Mo (VI) and W (VI) in water. *Talanta* **2013**, *105*, 80–86. [[CrossRef](#)]
24. Wu, P. *Anionic Clay Intercalation Construction and Environmental Remediation Technology*; Science Press: Beijing, China, 2016.
25. Chen, T.; Zhan, X.; Fan, M.; Chen, G.; Sun, J. Intercalation of pyrophosphate in the structure of anionic clay for instant synthesis. *Miner. Rock* **2005**, *76*, 105–108.
26. Türk, T.; Alp, İ.; Deveci, H. Adsorption of As (V) from water using Mg–Fe-based hydrotalcite (FeHT). *J. Hazard. Mater.* **2009**, *171*, 665–670. [[CrossRef](#)] [[PubMed](#)]
27. Yang, K.; Yan, L.G.; Yang, Y.M.; Yu, S.J.; Shan, R.R.; Yu, H.Q.; Zhu, B.C.; Du, B. Adsorptive removal of phosphate by Mg–Al and Zn–Al layered double hydroxides: Kinetics, isotherms and mechanisms. *Sep. Purif. Technol.* **2014**, *124*, 36–42. [[CrossRef](#)]
28. Liang, X.F.; Hou, W.G.; Xu, Y.M.; Sun, G.H.; Wang, L.; Sun, Y.; Qin, X. Sorption of lead ion by layered double hydroxide intercalated with diethylenetriaminepentaacetic acid. *Colloids Surf. a-Physicochem. Eng. Asp.* **2010**, *366*, 50–57. [[CrossRef](#)]
29. Wang, Y.; Ding, S.; Ren, M.; Li, C.; Xu, S.; Sun, Q.; Xu, L. Enhanced DGT capability for measurements of multiple types of analytes using synergistic effects among different binding agents. *Sci. Total Environ.* **2019**, *657*, 446–456. [[CrossRef](#)]
30. Hou, H.; Cui, W.; Xu, Q.; Tao, Z.; Guo, Y.; Deng, T. Arsenic Species Analysis at Trace Level by High Performance Liquid Chromatography with Inductively Coupled Plasma Mass Spectrometry. *Int. J. Anal. Chem.* **2019**, *4*, 1–6. [[CrossRef](#)]

31. Komorowicz, I.; Sajnóg, A.; Barańkiewicz, D. Total arsenic and arsenic species determination in freshwater fish by ICP-DRC-MS and HPLC/ICP-DRC-MS techniques. *Molecules* **2019**, *24*, 3. [[CrossRef](#)]
32. Morales, J.A.; de Graterol, L.S.; Mesa, J. Determination of chloride, sulfate and nitrate in groundwater samples by ion chromatography. *J. Chromatogr. A* **2000**, *884*, 185–190. [[CrossRef](#)]
33. Zhao, X.; Wang, H.; Tang, Z.; Zhao, T.; Qin, N.; Li, H.; Wu, F.; Giesy, J. Amendment of water quality standards in China: Viewpoint on strategic considerations. *Environ. Sci. Pollut. Res.* **2018**, *25*, 3078–3092. [[CrossRef](#)]
34. Wang, Y.; Ding, S.; Gong, M.; Xu, S.; Xu, W.; Zhang, C. Diffusion characteristics of agarose hydrogel used in diffusive gradients in thin films for measurements of cations and anions. *Anal. Chim. Acta* **2016**, *945*, 47–56. [[CrossRef](#)]
35. Guan, D.X.; He, S.X.; Li, G.; Teng, H.H.; Ma, L.Q. Application of diffusive gradients in thin-films technique for speciation, bioavailability, modeling and mapping of nutrients and contaminants in soils. *Crit. Rev. Environ. Sci. Technol.* **2021**, *1*, 1–45. [[CrossRef](#)]
36. He, S.; Wang, X.; Wu, X.; Yin, Y.; Ma, L.Q. Using rice as a remediating plant to deplete bioavailable arsenic from paddy soils. *Environ. Int.* **2020**, *141*, 105799. [[CrossRef](#)] [[PubMed](#)]
37. Ding, S.; Sun, Q.; Xu, D.; Jia, F.; He, X.; Zhang, C. High-resolution simultaneous measurements of dissolved reactive phosphorus and dissolved sulfide: The first observation of their simultaneous release in sediments. *Environ. Sci. Technol.* **2012**, *46*, 8297–8304. [[CrossRef](#)] [[PubMed](#)]
38. Teasdale, P.R.; Hayward, S.; Davison, W. In situ, High-Resolution Measurement of Dissolved Sulfide Using Diffusive Gradients in Thin Films with Computer-Imaging Densitometry. *Anal. Chem.* **1999**, *71*, 2186–2191. [[CrossRef](#)] [[PubMed](#)]
39. Guan, D.X.; Williams, P.N.; Xu, H.C.; Li, G.; Luo, J.; Ma, L.Q. High-resolution measurement and mapping of tungstate in waters, soils and sediments using the low-disturbance DGT sampling technique. *J. Hazard. Mater.* **2016**, *316*, 69–76. [[CrossRef](#)]
40. Liang, X.; Xu, Y.; Wang, L.; Sun, Y.; Lin, D.; Sun, Y.; Qin, X.; Wan, Q. Sorption of Pb<sup>2+</sup> on mercapto functionalized sepiolite. *Chemosphere* **2013**, *90*, 548–555. [[CrossRef](#)]
41. Criscenti, L.; Sverjensky, D. The role of electrolyte anions (ClO<sub>4</sub><sup>−</sup>, NO<sub>3</sub><sup>−</sup>, and Cl<sup>−</sup>) in divalent metal (M<sup>2+</sup>) adsorption on oxide and hydroxide surfaces in salt solutions. *Am. J. Sci.* **1999**, *299*, 828–899. [[CrossRef](#)]
42. Bennett, W.W.; Teasdale, P.R.; Panther, J.G.; Welsh, D.T.; Jolley, D.F. New diffusive gradients in a thin film technique for measuring inorganic arsenic and selenium(IV) using a titanium dioxide based adsorbent. *Anal. Chem.* **2010**, *82*, 7401–7407. [[CrossRef](#)]
43. Wang, Y.; Ding, S.; Shi, L.; Gong, M.; Xu, S.; Zhang, C. Simultaneous measurements of cations and anions using diffusive gradients in thin films with a ZrO-Chelex mixed binding layer. *Anal. Chim. Acta* **2017**, *972*, 1–11. [[CrossRef](#)] [[PubMed](#)]
44. Coyte, R.M.; Vengosh, A. Factors controlling the risks of co-occurrence of the redox-sensitive elements of arsenic, chromium, vanadium, and uranium in groundwater from the eastern United States. *Environ. Sci. Technol.* **2020**, *54*, 4367–4375. [[CrossRef](#)] [[PubMed](#)]
45. Puca, C.; Moldovan, M.; Silaghi-Dumitrescu, L.; Ungureanu, L.; Silaghi-Dumitrescu, R. On the apparent redox reactivity of “oxygen-enriched water”. *Biol. Trace Elem. Res.* **2020**, *198*, 350–358.
46. Yan, Y.; Qian, Y.; Wang, Z.Y.; Yang, X.Y.; Wang, H.W. Ecological risk assessment from the viewpoint of surface water pollution in Xiamen City, China. *Int. J. Sustain. Dev. World Ecol.* **2018**, *25*, 403–410. [[CrossRef](#)]
47. Coffin, M.; Courtenay, S.C.; Pater, C.C.; Heuvel, M. An empirical model using dissolved oxygen as an indicator for eutrophication at a regional scale. *Mar. Pollut. Bull.* **2018**, *133*, 261–270. [[CrossRef](#)]
48. Jiang, M.; Sheng, Y.; Liu, Q.; Wang, W.; Liu, X. Conversion mechanisms between organic sulfur and inorganic sulfur in surface sediments in coastal rivers. *Sci. Total Environ.* **2020**, *752*, 141829. [[CrossRef](#)]
49. Wu, B.; Liu, F.; Fang, W.; Yang, T.; Wang, S. Microbial Sulfur metabolism and environmental implications. *Sci. Total Environ.* **2021**, *778*, 146085. [[CrossRef](#)]
50. Armstrong, J.; Armstrong, W. Rice: Sulfide-induced barriers to root radial oxygen loss, fesu2plus/sup and water uptake, and lateral root emergence. *Ann. Bot.* **2005**, *96*, 625–638. [[CrossRef](#)]
51. Xu, C.; Chen, L.; Chen, S.; Chun, G.; Wang, D.; Zhang, X. Effects of rhizosphere oxygen concentration on root physiological characteristics and anatomical structure at the tillering stage of rice. *Ann. Appl. Biol.* **2020**, *177*, 61–73. [[CrossRef](#)]
52. Wu, Z.Y.; Zhang, C.H.; Yan, J.L.; Yue, Q.; Ge, Y. Effects of sulfur supply and hydrogen peroxide pretreatment on the responses by rice under cadmium stress. *Plant Growth Regul.* **2015**, *77*, 299–306. [[CrossRef](#)]
53. Zhang, D.; Du, G.; Chen, D.; Shi, G.; Rao, W.; Li, X.; Jiang, Y.; Liu, S.; Wang, D. Effect of elemental sulfur and gypsum application on the bioavailability and redistribution of cadmium during rice growth. *Sci. Total Environ.* **2019**, *657*, 1460–1467. [[CrossRef](#)] [[PubMed](#)]